ELSEVIER

Journal of Structural Geology 27 (2005) 2281–2300

JOURNAL OF STRUCTURAL GEOLOGY

www.elsevier.com/locate/jsg

Processes of normal fault evolution in a siliciclastic sequence: a case study from Miri, Sarawak, Malaysia

Wouter van der Zee*, Janos L. Urai

Geologie-Endogene Dynamik, RWTH Aachen, Germany

Received 14 June 2004; received in revised form 6 June 2005; accepted 4 July 2005
Available online 15 September 2005

Abstract

Detailed field observations of normal faults formed at shallow depth in a deltaic sand–clay sequence near Miri, Sarawak are used to study the main structural elements during the early stages of fault development. We studied over 450 segmented faults, many of which contain clay smear, in an excellent outcrop exposing a collapsed crest structure.

In agreement with previous studies we find that important elements of fault zone evolution are: (i) clay smear, (ii) telescoping on parallel strands, and (iii) preferred deformation of fault-bounded lenses. We model the consequences of telescoping on parallel strands and conclude that the reliability of juxtaposition diagrams can decrease dramatically in the presence of undetected multiple fault strands. The across fault connectivity can either increase or decrease depending on small variations in many of the input parameters.

All the faults studied have a continuous clay smear over the interval studied, except for the places where a sand bed has an offset smaller than its thickness, and therefore has not moved past clay. Although on average the clay content observed correlates well with the average clay content of the faulted section, there are large variations in clay content controlled by local complexity in deformation. Understanding of this local complexity is a prerequisite for further improvement of clay smear in the subsurface.
© 2005 Elsevier Ltd. All rights reserved.

Keywords: Faults; Clay smear; Field observations

1. Introduction

This paper presents a study of normal fault zones in layered siliciclastic sediments deformed at a depth of less than 1000 m. Fault zones are usually the sites of large discontinuous changes in mechanical and transport properties (Bense et al., 2003a; Vrolijk et al., 2005) which are controlled by the composition and structure of the fault gouge. In faults of large offset, the structure of 'mature' fault gouges has been described by several workers (Chester and Logan, 1986; Chester and Chester, 1998; Snoke et al., 1998; Wibberley and Shimamoto, 2003). The early development of fault gouges starting from the initial discontinuities is less well known. Understanding this early, transient stage is important for several reasons. First, because most mature fault gouges have passed through this stage, interpreting the evolution of mature faults is aided by an understanding of processes during the early stages of evolution. Second, in faulted areas one always finds faults with small throw, in isolated small faults or at the tips of large faults. Finally, the changes in mechanical properties of a rock body caused by a fault are the largest in the early stages of faulting.

Research on the early development of fault gouges has so far mainly concentrated on faults in thick layers and thus single phase materials. In such cases, dependent on lithology and environmental parameters (effective stress, temperature, etc.), a range of grain-scale processes has been documented. Examples are grain sliding or cataclasis with possible diagenesis in sand(stone), and associated changes in porosity and permeability (Antonelli and Aydin, 1995; Fulljames et al., 1997; Knipe et al., 1997), pressure solution, cataclasis, vein development and jointing in chalk and limestone (Peacock and Sanderson, 1994; Childs et al., 1996a; Willemse et al., 1997) and the formation of shear zones by grain sliding and crystal plasticity or cataclasis in mudstones (Morgenstern and Tshalenko, 1967; Maltman,

* Corresponding author. Present address: GeoMechanics International, Mainz, Germany. Tel.: +49 61316272814; fax: +49 61316272829.
E-mail address: zee@geomi.com (W. van der Zee).

0191-8141/$ - see front matter © 2005 Elsevier Ltd. All rights reserved.
doi:10.1016/j.jsg.2005.07.006

1987; Urai and Wong, 1994; Urai, 1995; Holland et al., 2003; Hoogerduin-Strating and Urai, 2003).

At a larger scale, a variety of investigations of fault zone architecture were reported, ranging from mapping of deformation band networks in sandstone (Antonelli and Aydin, 1995), measurement of fault densities in damage zones (McGrath and Davison, 1995; Beach et al., 1999), to mapping of faults using seismic data (Mansfield and Cartwright, 1996; Morley and Burhanndinnur, 1997). The statistics of geometric relationships are reviewed by Childs et al. (1990), Walsh and Watterson (1993) and Yielding et al. (1996). A review paper summarizing the nomenclature used for normal faulting is given by Peacock et al. (2000).

The general picture emerging is that of a set of initial discontinuities (simple deformation bands (Mühlhaus and Vardoulakis, 1987) or joints (Bürgmann and Pollard, 1994)), which upon further deformation propagate and organize into a fault zone (Crider and Peacock, 2004). Further deformation is accommodated by linkage of the segments and deformation of the relays and asperities (Childs et al., 1996a; Willemse, 1996). With progressive shearing the material in this zone becomes deformed so strongly that initial structure is largely obliterated by mechanical mixing, (Heynekamp et al., 1999; Vrolijk and van der Pluijm, 1999). At this stage the fault zone can only partly be restored to its equivalent in the wall rock. Such zones are also called a 'mature' gouge, in which a central fault core and a surrounding damage zone can often be distinguished. The zone of mature gouge contains the fault core. It is often possible to distinguish the 'initial structure' preserved in the damage zone once slip has been localized in the fault core—though this is likely to be highly dependent on the fault history and host rock lithology (Chester and Logan, 1986; Caine et al., 1996). Several studies report an increase in degree of deformation near such faults (McGrath and Davison, 1995; Scruggs and Tullis, 1998; Beach et al., 1999; Wibberley and Shimamoto, 2003).

Less is known of the development of fault zones in layered sequences, although the majority of relevant settings are layered. Layering is expected to introduce additional complexity because of the contrast in strength and transport properties between the layers. Some outcrop work is reported from research in chalk and marls (Peacock and Sanderson, 1994; Childs et al., 1996a), and sand and clay (Burhanndinnur and Morley, 1997; Lehner and Pilaar, 1997; Heynekamp et al., 1999; van der Zee, 2002; Bense et al., 2003b; Clausen et al., 2003).

A model of lateral clay injection into faults in unconsolidated sand–clay multilayers was proposed by Lehner and Pilaar (1997) and van der Zee et al. (2003) who described the kinematics and mechanics of the process. In hard overconsolidated shales, Lindsay et al. (1993) analyzed the clay abrasion process that produces a clay gouge composed of softened and reworked clay from the over-consolidated host mudstone.

For faults in sand–mudstone sequences much of the research is focused on predicting the amount of clay incorporated into the fault gouge, often called 'clay-smear'. In hydrocarbon geology, understanding these processes is important for the prediction of fault sealing (Weber et al., 1978; Lindsay et al., 1993). For applied studies of fault seal evaluation, a number of semi-empirical tools were developed. An overview and comparison of these methods: clay smear potential (Bouvier et al., 1989; Fulljames et al., 1997), shale smear factor (Lindsay et al., 1993) and shale gouge ratio (Fristad et al., 1997; Yielding, 2002) is given by Yielding et al. (1997).

Our study aims at describing the processes during fault

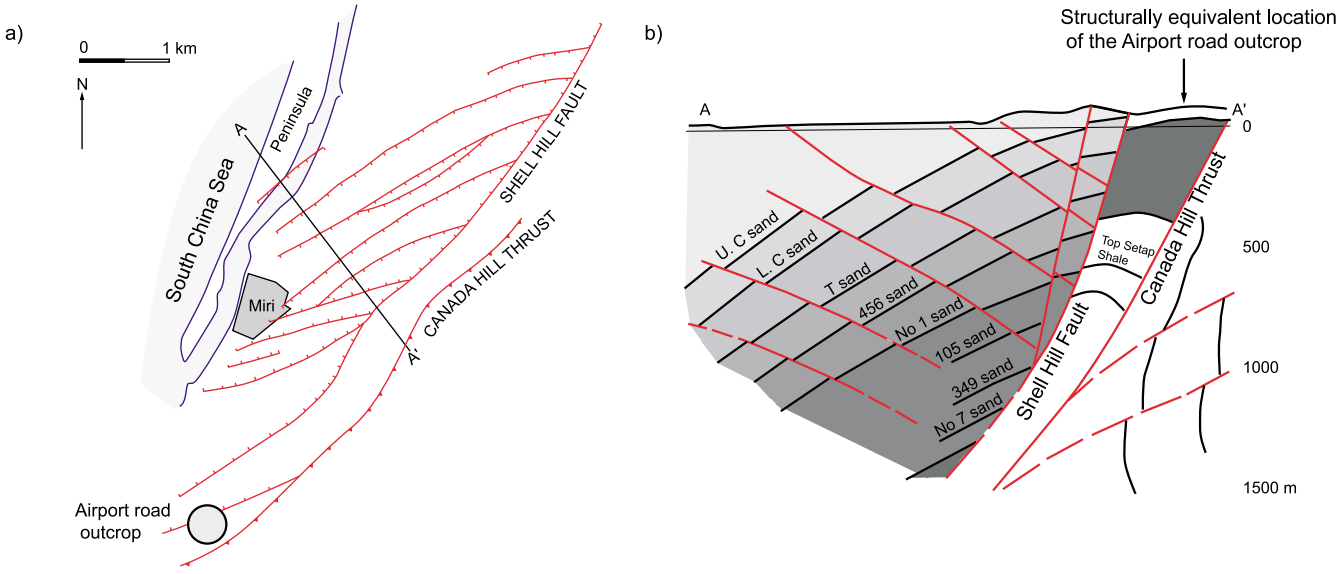

Fig. 1. (a) Tectonic map of the area with the main faults identified, and the location of the Airport road outcrop (after SSB fieldtrip handout). (b) Cross-section of the Miri structure.

zone development in a layered siliciclastic sequence, from single deformation bands to a mature fault zone. In this paper we present results of detailed field observations on well-exposed fault systems in an outcrop near Miri, Malaysia. From these observations, we attempt to identify the key elements of structural evolution, and discuss some aspects relevant to the transport properties of such zones. We present a probabilistic model of the effect of the complexity of the fault zone on transport properties, and a geomechanical model to explain the partitioning of deformation observed in some of the structures.

2. Geological setting

We studied excellent outcrops of normal faults in layered deltaic sediments along the Airport road near Miri, Malaysia (coordinates: N04°21′50″/E113°58′45″). This outcrop was

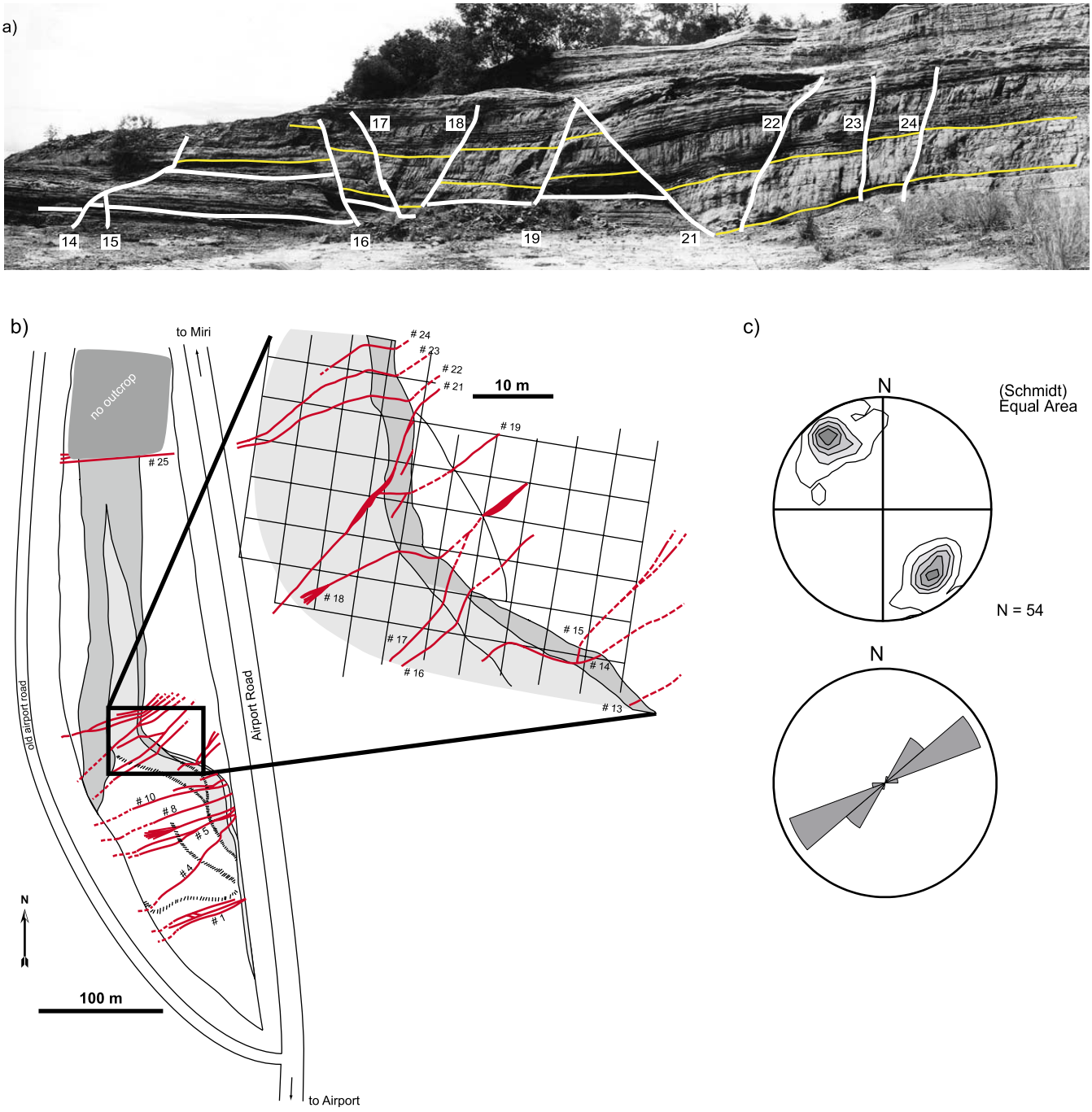

Fig. 2. (a) Overview of the central part of the outcrop. The larger faults are indicated and numbered. (b) Fault map of the Airport road outcrop, including enlargement of the central part. Sharp changes in fault orientation are due to topography. The total elevation difference in the outcrop is 30 m. Faults are numbered for reference in the text. (c) Stereoplots of the orientations of the main faults (lower hemisphere, equal area).

previously documented by Lesslar and Wannier (1998) and Burhanndinnur and Morley (1997).

Stratigraphically the rocks belong to the Miocene 456 Sands of the Miri formation; a stack of deltaic cycles forming a layered clay–sand sequence (85% sand and 15% clay) with laterally discontinuous sand bodies. Most clay layers are thin (~10 cm), with a small number of thicker layers up to 50 cm thick. Therefore this sequence is sufficiently thin-bedded to form faults with throws more than 10 times the layer thickness. This allows the study of the 'complete fault', i.e. one with the faulted layers outcropping on both sides of the faults.

The outcrop is situated in the same structure as the Miri oilfield which was producing from 1910 to 1979. The Airport road outcrop is interpreted as an exhumed part of a collapsed crest anticline between the Shell Hill Fault in the north and the Canada Hill Thrust in the south (Fig. 1a). Although the details of the large scale kinematics are not known, the location between a large normal fault and a large thrust resulted in the uplift of a 'slice' of reservoir rock (Fig. 1b). The major deformation is extensional, which produced abundant normal faults. Signs of the complex strike–slip and reverse faulting of the Miri structure are rare in the outcrop in the form of small reverse and strike–slip faults.

The main deformation in the Airport road outcrop occurred in an extensional setting after burial to depths less than 1000 m, as indicated by clay porosity, the almost complete absence of cataclasis in sand, and vitrinite reflectance in rare coal layers (Schmitz et al., 2003). Cementation was mild if any, and possibly occurred after deformation.

3. Methodology

Most surfaces of the Airport road outcrop are clean, exposing in 3D a system of over 450 normal faults with throws ranging from several centimeters to over 25 m (Fig. 2a). The sandstone and clays in the outcrop can be classified as soft rocks. In critical areas, where outcrop is not 100% this allows preparation of smooth clean surfaces with detail visible down to the millimeter scale, with hand tools.

We identified the major sedimentary and structural elements in the outcrop. All fault structures were mapped at a scale of 1:50, both in plane and in profile. For mapping, the horizontal part of the outcrop was covered with a 5 m × 5 m mesh. In these, the main structural elements were measured and plotted. These maps (Fig. 2b) in combination with data from the vertical outcrop faces allowed study of the 3D fault structure.

The structures were photographed at different scales, carefully avoiding distortion as much as possible, and in a direction parallel to critical structural elements such as the local fault plane. This produced a database of over 1000 high-resolution images. Interpretation was done using these high-resolution photographs (as shown in many figures, e.g. Figs. 5, 10 and 14).

To collect an as complete as possible dataset of the fault structures, the following measurement strategies were used:

- Scanlines were laid out perpendicular to the main fault strike, along a vertical part of the outcrop, following a layer along the outcrop face. Structural elements such as orientation, displacement, spacing, fault length, etc. were measured. This dataset of a total of 90 m is complete (sampled in 100% outcrop). All structures (down to millimeter scale) that were visible to the naked eye were logged. Intervals logged as containing no faults are free of deformation features larger than 1 mm displacement.
- In addition, measurements were done along selected fault planes, in both horizontal and vertical sections. We logged the number of fault strands, and measured the fault width, clay thickness of the fault gouge, offset (only in vertical section), and strike of the fault segments (only in horizontal section).

4. Fault geometry

In the outcrop bedding is sub-horizontal, with no dip larger than 10°. The faults strike perpendicular to the main outcrop faces, the average fault strike is 052–232°. The fault plane orientations show two maxima: the north-dipping faults have an average orientation of 324/61, while the south-dipping faults have an average orientation of 143/72 (Fig. 2c).

Most of the structural elements connected with faults were found to occur at a range of scales (Neugebauer, 2003). In what follows we describe the most important elements in the outcrop.

Differences in layer thickness occur across some of the faults. These could be interpreted as evidence for growth faulting. However, the variations are not systematic, and the magnitude is never more than could be expected based on the lateral variation in layer thickness in unfaulted parts of the outcrop. This is a common feature in deltaic settings. Therefore we interpret the faults to have formed after sedimentation and burial.

4.1. Deformation bands

Deformation bands are thin (a few millimeters wide) zones of highly localized deformation, with usually less than a few mm displacement. They are considered to be basic building blocks of fault zones in many porous, previously undeformed siliciclastics (Antonelli and Aydin, 1995; Ingram and Urai, 1999). Usually they are interpreted to represent pre-cursor deformation in a work-hardening stage before deformation becomes generally localized onto

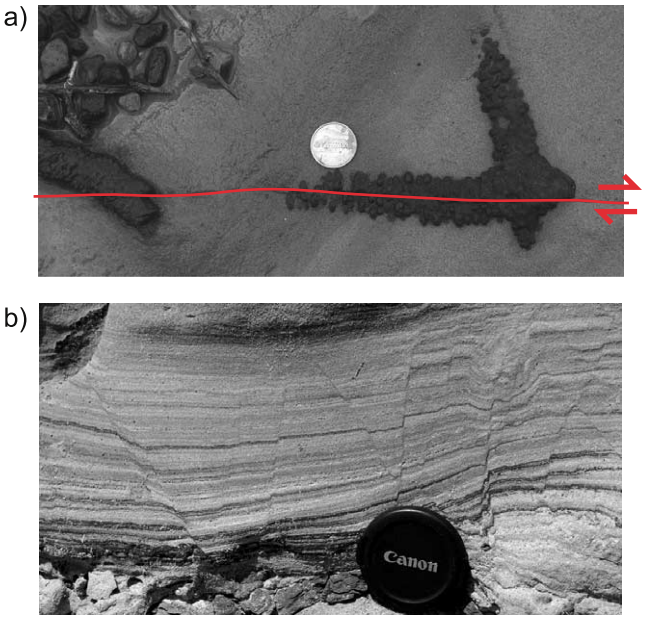

Fig. 3. (a) Strike–slip component of offset of a deformation band crosscutting an oxide-decorated burrow. The photograph was taken looking down on a horizontal outcrop surface. Coin for scale. (b) Set of deformation bands with offsets ranging from 1 to 5 mm. Lens cap for scale.

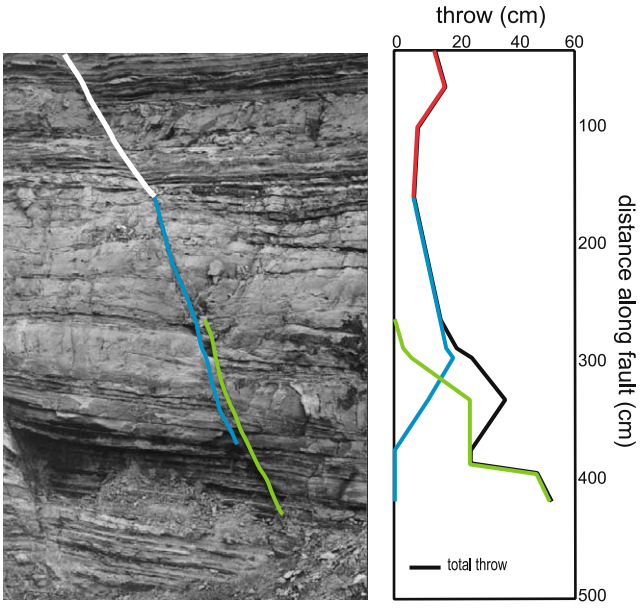

Fig. 4. Fault 17 in a 5 m high vertical outcrop. Three main segments can be recognized. This is illustrated by the throw profile along the fault dip, which has three distinct maxima.

throughgoing faults. In our dataset, single deformation bands only rarely have microscopic evidence for cataclasis, and have the typical macroscopic morphology documented in previous works (Antonelli and Aydin, 1995). They usually have displacements of a few millimeters, sometimes up to 1 cm (Fig. 3b). Occasionally, oxide-decorated burrows provide a possibility of determining the true displacement vector of the deformation bands. Movement direction is down-dip, with rarely (cf. Fig. 3a) a strike–slip component.

4.2. Joints

Several authors reported joints as initial discontinuities (Bürgmann and Pollard, 1994; Martel, 1999) from which a

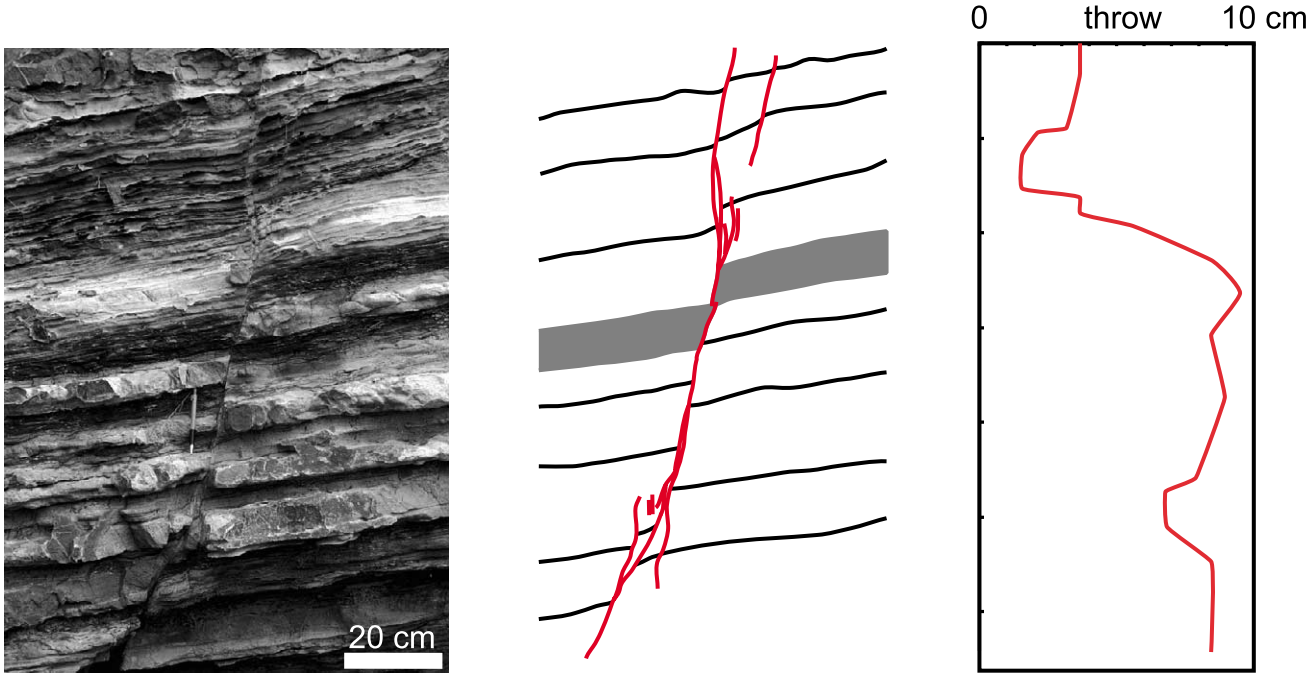

Fig. 5. Fault 7 shows an irregular displacement profile. The fault consists of several non co-planar coalesced segments. The linkage produced a releasing (near the top) and restraining (near the bottom) bend. Additional deformation is observed near these bends.

fault zone evolves. These, usually bedding-perpendicular, joints can have a large influence on the shape of the future fault. In the Airport road outcrop some sandstone beds have a well-developed joint pattern. The average strike of these joints is 035–215°. The large majority of these joints do not show any movement along the joint surface, reactivated joints are rare. We interpret the joints as late features, absent during the main (extensional) phase of deformation.

4.3. Segmented faults

Widespread evidence has been documented that fault growth occurs by coalescence of segments, horizontally (Cartwright et al., 1996; Willemse and Pollard, 2000) and vertically (Childs et al., 1996b; Mansfield and Cartwright, 1996). At larger offset the initial discontinuities increase in number and reorganize into a network of strands that can be considered a single fault (Burhanndinnur and Morley, 1997). Our observations are consistent with this general notion. Almost all of the faults studied (we use the term fault for structures with offsets above a few centimeters) are segmented, as shown by the displacement profile (Figs. 4 and 5). The segments do not necessarily have the same orientation or are in the same plane. This causes structures such as soft-linkage and short-cut faults, and results in an increase of complexity and in a local widening of the fault zone, similar to the structures described by Childs et al. (1996a).

In the segments of faults with an offset more than a meter, the fault gouge usually consists of several anastomozing strands. Fig. 6 shows such a complex clay-rich gouge in a fault with an offset of 2.5 m, in a sequence with many thin clay and sand layers. One can see the sharp transition from country rock to fault zone. Coherency is lost between source beds (following the layers into the fault is not possible based on visual observation), and the sheared clay and sand develops into a foliated fault gouge.

The zone with three larger faults in the outcrop (fault 25, see Fig. 2b, estimated displacement between 25 and 100 m) shows a complex layered structure of the fault gouge. These mature gouges have a layer of clay rich gouge in the center next to a mixed sand–clay zone with a high density of small faults beside it (Fig. 7; Rawling et al., 2001). Because these faults do not allow tracing of source beds from one side of the fault to the other (offset more than height of the outcrop), this paper concentrates on the other faults shown in Fig. 2b.

In summary, the coalescence of non co-planar segments or segments with non-uniform orientation produces zones of increased complexity. These points have the highest variety in structure, and a large influence on the overall architecture of the fault. Interesting features such as short-cut faults, branches (Fig. 8) and slip plane bounded lens shaped bodies (Fig. 9) are mostly found at these coalescence points.

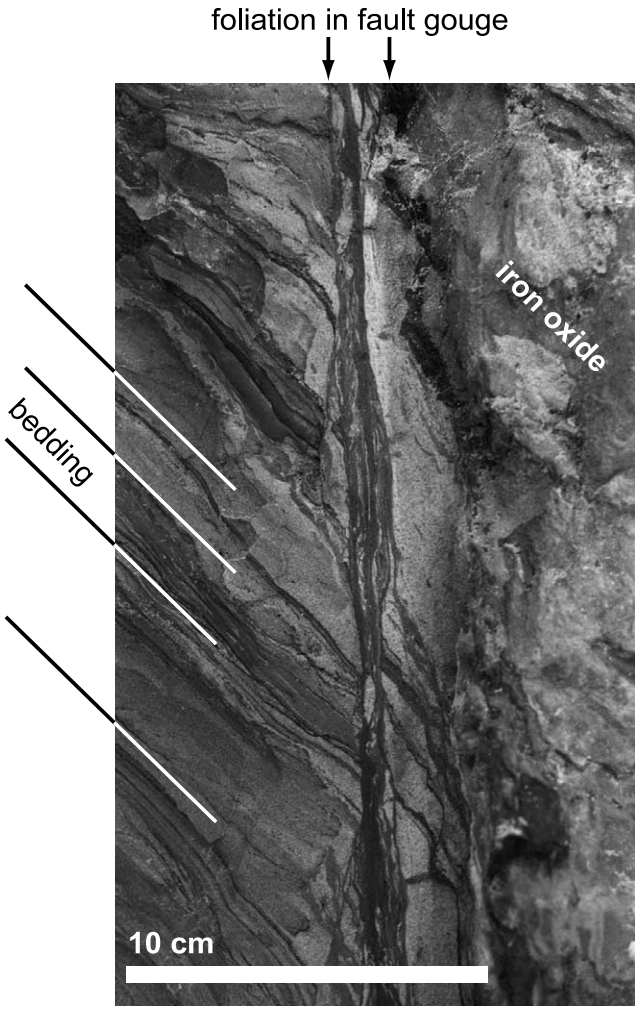

Fig. 6. Close-up of a network of deformation bands in fault 16, which has a throw of 2.5 m. The picture is taken parallel to fault strike; the long axis of the photo is parallel to the fault dip direction, therefore the horizontal bedding is shown with an angle on the photograph. The fault was cleaned to allow high resolution observations. One cannot follow the beds from the wall rock into the fault zone. The sheared sand and clay in the fault develop into a foliated gouge. On the right side of the fault zone cleaning was not possible due to the presence of a hard oxide layer, which presumably formed as a weathering product from groundwater flowing downwards along the right side of this sealing fault.

4.4. Fault-bounded lens shaped bodies

Fault-bounded lens shaped bodies in a fault zone are commonly observed features (Ramsay and Huber, 1987; Childs et al., 1996a, 1997; Walsh et al., 1999). These are relatively common in the Airport road outcrop, and occur at different scales. Our observations show that the lenses are always deformed stronger than the material outside it. To quantify this degree of deformation, we measured (i) deformation band density and (ii) tilt of the bedding along scanlines across the lenses. Fig. 9 is an example of the results for a lens in fault 10. The graph of deformation band

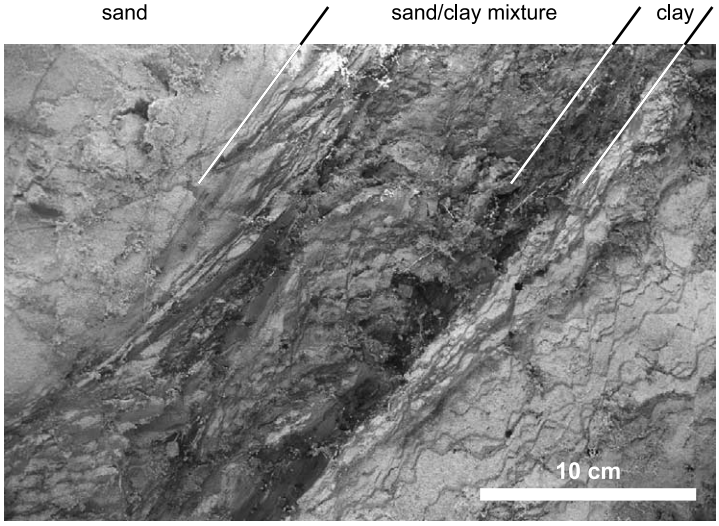

Fig. 7. Close-up of the mature fault gouge in fault 25. This fault has a displacement of more than the outcrop height, but less than the thickness of the 456 sands (150 m). The gouge consists of a 10-cm-thick clay-rich zone in the middle with, on both sides, a mixed sand–clay zone with a high density of Riedel shears.

density averaged over 10 cm intervals shows a clear increase inside the lens. The bedding shows only a small increase in dip in the center of the lens, but a significant increase in the lens tip. We interpret these data to indicate a stronger deformation inside the lens, either by movement along multiple deformation bands or by layer-parallel shear. The mechanics of such fault-bounded lenses are further explored using a geomechanical model. Results of this are presented later in Ch 7 of this paper.

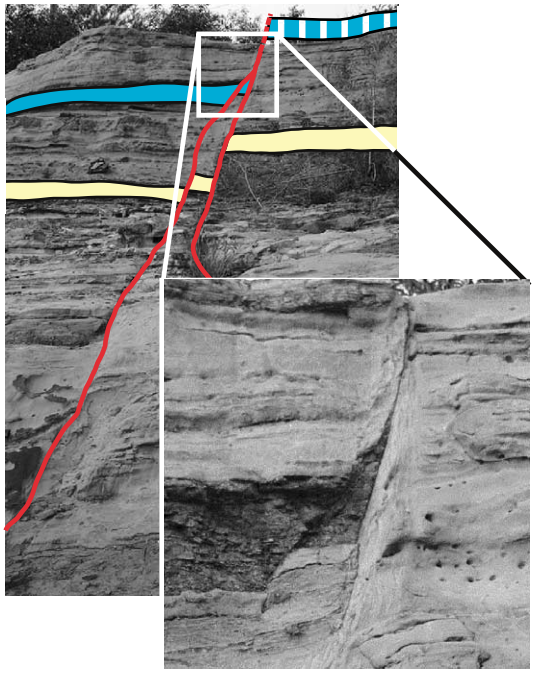

Fig. 8. Coalescence of two sub-parallel faults (faults 22 and 23; see Fig. 2a). The zone around the linkage point is strongly deformed as shown by the increasing density of deformation bands. The enlargement shows the structure at this linkage point.

4.5. Fault with multiple slip planes

Faults containing multiple parallel slip planes were identified by several authors (Childs et al., 1996a, 1997). Such structures are commonly observed in the outcrop, in zones of segment linkage, and near restraining bends. Fig. 10a shows a fault structure consisting of four parallel strands that are recognizable by the offset of the base of the sand bed. Detailed observation shows that deformation of the clay is concentrated in four thin zones. We interpret the thick clay between the sand beds to be a result of 'tectonic telescoping' along parallel strands, and not as a thick clay gouge. This is illustrated by a kinematic reconstruction shown in Fig. 10b. It is clear that this tectonic telescoping has a large influence on across fault juxtaposition and hydraulic connectivity (Childs et al., 1997).

4.6. Fault statistics

4.6.1. Distribution of length and throw

Statistical properties of the fault system were investigated by measurements of fault length (defined as the vertical length in the outcrop face) and fault throw along two scanlines with a cumulative length of 90 m, along a thin coal bed. Fig. 11a shows the cumulative number vs. throw and a cumulative number vs. length plot. The very good correlation in this log–log diagram supports the interpretation of the system as a fractal set, with a (1D) fractal dimension comparable with those reported by Yielding et al. (1996).

The low and high sides of the data show some deviation from linearity. For the large faults this is due to the limited vertical size of the outcrop. (Faults with a length longer than 30 m are longer than the height of the outcrop; for these we used a length value of 30 m.) On the other hand, we argue that the smallest faults shown in the diagrams represent the

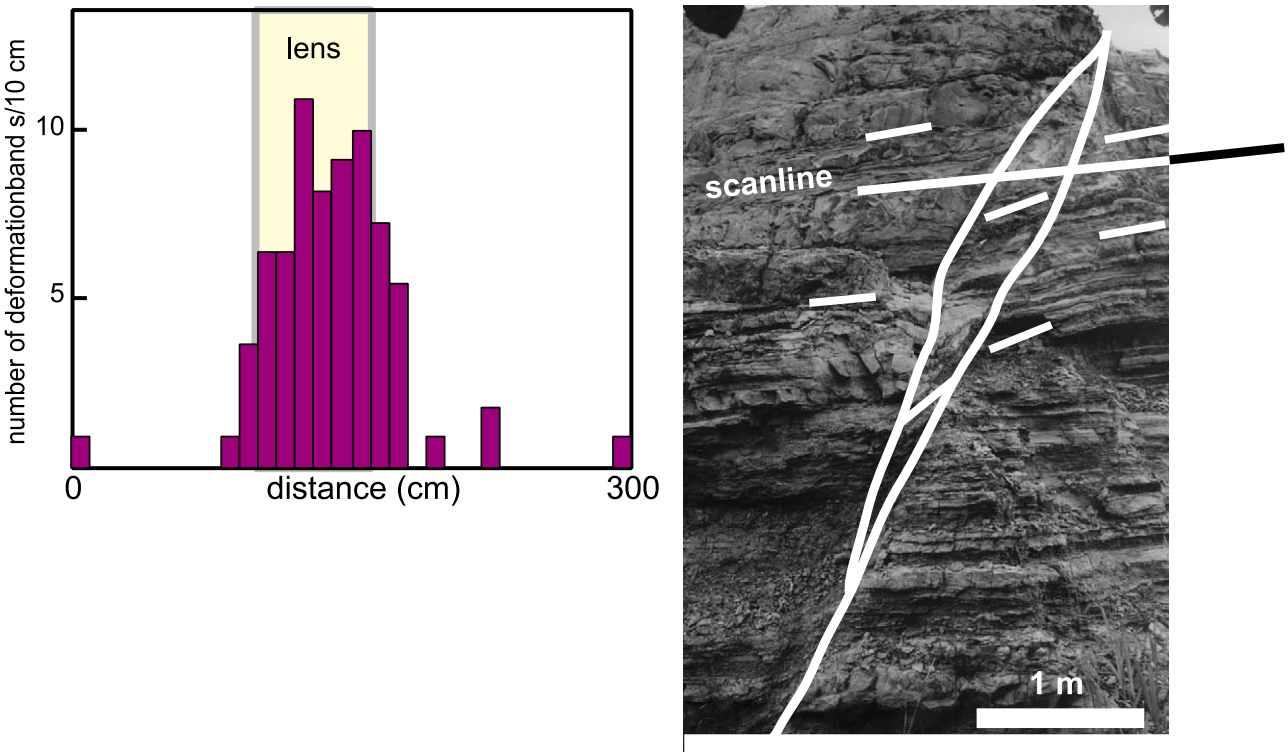

Fig. 9. Deformation band density for 10 cm intervals along a scanline through a fault-bounded lens shaped structure in fault 10. Clearly visible is the higher density inside the lens. Small white bars are indicators for dip of bedding. Note that the bedding shows only a small increase in dip in the center of the lens, but a significant increase in the lens tip.

lower limit of the fractal system for this outcrop, because faults with throws smaller than 1 mm are not recognizable (the grain size of the sand is of the order of 0.2 mm).

4.6.2. Fault profile roughness

The clean horizontal faces of the outcrop allowed continuous observations along strike for several faults. To measure the roughness of the fault profile, the orientations of 50 cm segments along the fault strike are measured. This was done by laying out a measuring-tape as straight as possible along the average strike of the fault. For every 50 cm along this tape, the corresponding orientation of the fault was recorded. Results of these measurements are shown in Fig. 11b. We analyzed the effect of small errors caused by topographical effects and the slight deviation from perfect linearity of the measuring-tape, and have shown that the effect of this error is negligible in the analysis of the roughness of the fault profile reported below.

The roughness of a fault profile (Navarro, 2002) is important because it affects shear strength: the rougher the fault, the larger the shear strength of the fault zone. The non-planar origin of the fault segments means that further displacement is only possible when asperities in the wallrock deform also. Fractals were shown to be very useful in characterizing rough surfaces (Brown and Scholz, 1985; Power and Tullis, 1991; Develi and Babadagli, 1998). We used the semi-variogram method because this method is useful for self-affine surfaces such as fracture and fault profiles (Develi and Babadagli, 1998). We analyzed three faults (Fig. 11c) and all three show good correlation in the double-logarithmic variogram vs. window width plot ($R^2 = 0.99$). The fractal dimensions vary between 1.14 and 1.24 for these 1D profiles.

4.7. Discussion of fault zone evolution

Based on the observations presented above, we interpret the structures in the Airport road outcrop to have formed during normal faulting (in a collapsed crest structure), relatively undisturbed by the exhumation process. The major part of the faulting occurred after burial at less than 1 km depth, as shown by the absence of cataclasis in the majority of the deformation bands, and by the absence of growth on all investigated faults. The exact timing of deformation during the burial is difficult to estimate, because the data available only measure maximum burial depth and maximum depth of faulting.

The structures observed have many aspects in common with the current models for fault development (Cartwright et al., 1996; Willemse and Pollard, 2000). In our case the deformation bands are the initially unconnected discontinuities from which the fault zones develop. The joints present in the outcrop are interpreted to be later than the faulting. We interpret the majority of these discontinuities to have nucleated inside the rock volume studied, and not propagated from outside (e.g. driven by a basement fault in

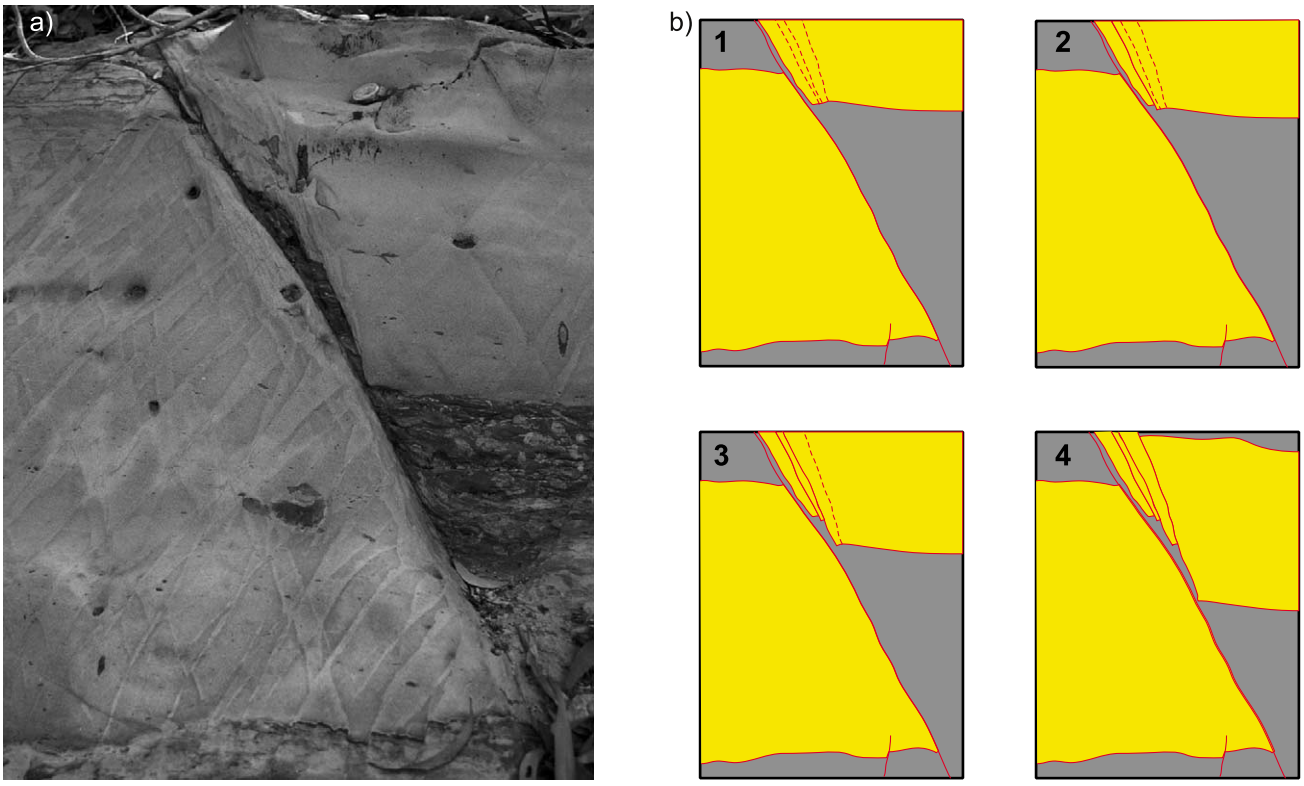

Fig. 10. An example of telescoping along parallel strands in fault 21. A kinematic reconstruction (interpreted time sequence 1–4) shows how this structure developed by the slip on four parallel strands. Note that the timing of the generation of the different parallel strands is not known, and this is one of a number of possible reconstructions.

the subsurface). This is in agreement with the collapsed crest setting.

When the coalescing segments are not co-planar, complex structures such as soft linkage, bends in the fault plane, multiple fault strands, fault-bounded lenses etc. are formed. Movement along these complexities causes additional deformation of the wall rock, development of new (short-cutting) faults and further incorporation of the wall rock into the fault zone. All these structures have a strong effect on the shape and irregularity of the array, and the fault zone has a strongly variable thickness, both along strike and down-dip.

Important structural processes in this evolution are (i) 'clay smear', (ii) telescoping on parallel strands and (iii) preferred deformation of fault-bounded lenses. In what follows, we discuss the process of telescoping on parallel strands and the preferred deformation of fault bounded lenses in greater detail.

5. 'Clay smear'

Clay smear is a loosely defined term in hydrocarbon geology. In the most general meaning, the term includes all processes that somehow transform clay in the wall rock into clay in the fault. All the structures described above can contribute to the development of clay smear. In what follows we discuss additional observations relevant to the incorporation of clay in the fault zone.

5.1. Continuity of clay seams in the fault

All faults that offset a clay layer more than a bed thickness contain a zone of clay in the fault gouge. This can be very thin, but is continuous at the scale down to the resolution of a hand lens. In other words, these clay seams were never found 'breached' in our observations. We have not found an exception to this observation in the outcrop, for faults observed in profile, even when offsetting single clay layers with up to 50 times the layer thickness. An example of this is given in Fig. 12.

The full 3D continuity of such clay seams is less easily tested in outcrop. In horizontal sections, the lateral termination of a clay gouge was observed a number of times. However, because in these sections information on fault throw is only available indirectly, a cause of this by the absence of offset clay on both sides cannot be excluded.

5.2. Lateral injection

One of the processes that locally enriches clay in the fault gouge is lateral injection, first described by Lehner and Pilaar (1997). In this process, the clay is soft enough to be squeezed out of a source bed into a releasing bend in the

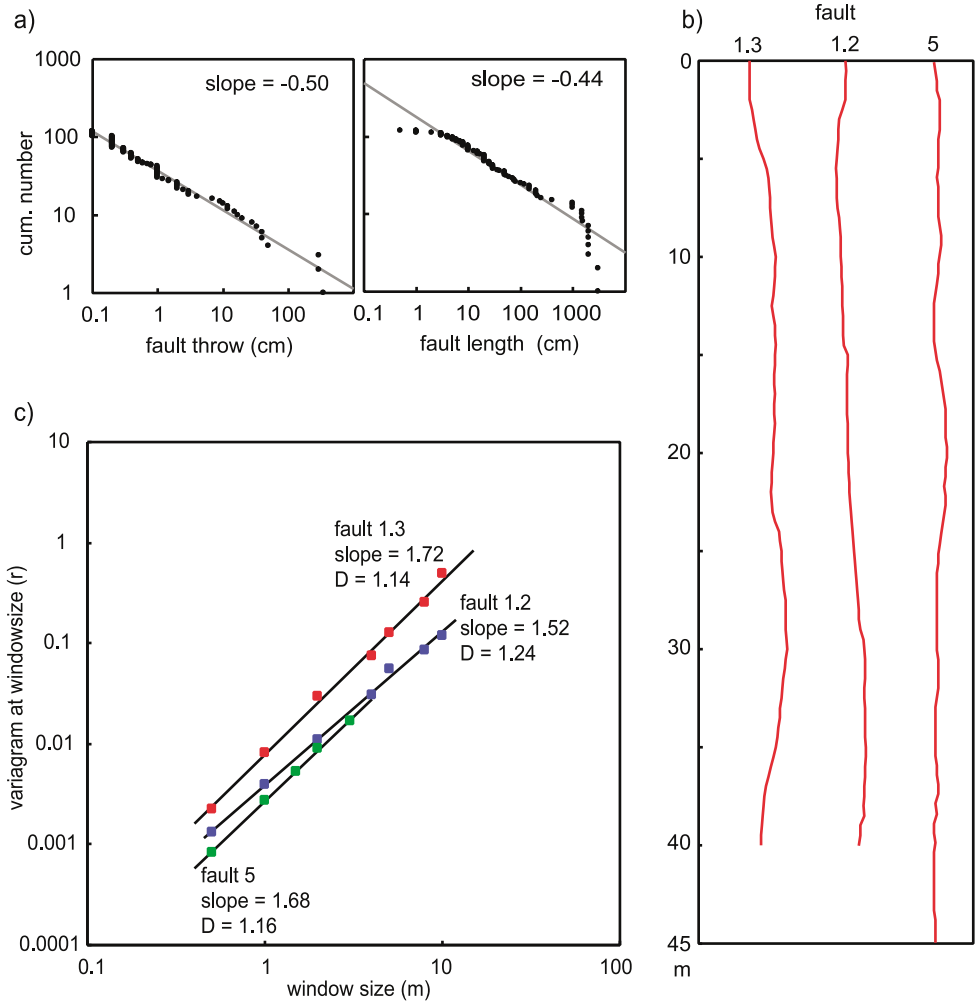

Fig. 11. Fault statistics. (a) Distribution of length and throw along two scanlines, showing 1D fractal dimensions of −0.5 and −0.44, respectively. (b) Map based on the orientation measurements in 50 cm intervals along three faults. (The sharp bends in the profile are due to topographical effects. Sensitivity analyses showed that the influence of these on the results in (c) is small). (c) Diagrams showing fault roughness with fractal dimensions between 1.14 and 1.24.

fault. Fig. 13 is a small-scale example of this. The clay bed of a few centimeters is stepwise thinned towards the main fault. The clay undergoes very high local deformation, which causes it to be reallocated into the fault. The lower sandstone bed is broken up, and a part of it is surrounded by the clay. Detailed study of the mechanics and kinematics of this process is reported in van der Zee et al. (2003).

5.3. Complex structures

The picture in Fig. 14 shows a close-up of fault 8. The clay layers are highly deformed and coalesce into one band. No sand is present in this part of the fault gouge. A detailed interpretation of the formation of this structure is difficult. It could be partly due to the lateral injection process. However, there are no clear signs of deformation or thickness changes in the clay layers that would indicate lateral extrusion (the apparent, small thickness changes in Fig. 14 are due to non-planar outcrop).

An alternative process is the breaking of the sandstone, combined with a shearing of the clay layer. This results in a faulted layered package where the different clay beds are dragged into the fault, and form a clay membrane in the fault gouge, whereas the sandstone did not shear and is therefore not present in the fault gouge. This absence of the sand causes the clay to coalesce into a clay-rich gouge. We introduce the term “preferred smear” for this process in this paper to indicate the enrichment of one of the wall rock constituents in the fault gouge.

In complex structures such as this one it can be expected that several processes operate in combination. In the resulting structure it is very difficult to separate the contributions of each process.

5.4. Clay gouge thickness vs. shale gouge ratio

Four faults (faults 13–16) in the vertical outcrop offered the possibility to make accurate measurements of throw, fault gouge structure (clay thickness, fault zone width, percentage of clay in the gouge), bed thickness and

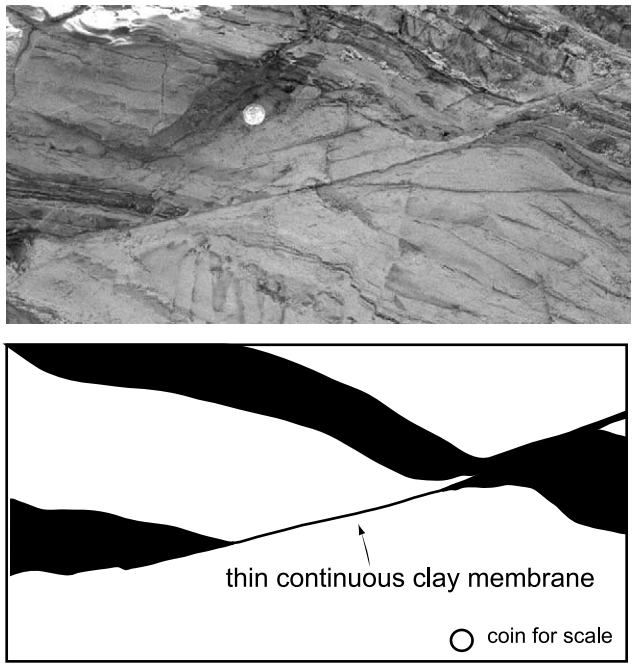

Fig. 12. Photograph of a small fault from the damage zone of fault 25. The outcrop face is at a 45° angle with fault strike, which is the reason for the low (apparent) dip on the photo. A clay layer is offset and sheared, forming a thin but continuous clay gouge between two sandstones.

lithology. This dataset was used to calculate the shale gouge ratio (SGR; Fristad et al., 1997; Yielding, 2002) in profile along the fault. The shale gouge ratio of a point on the fault is the ratio of clay to sand of the material that passed this point during faulting.

Fig. 15 shows a plot of the results for faults 13 and 16. Fault 13 has a throw between 20 and 30 cm and the studied interval contains about 70% sand. Fault 16 has a fairly constant throw of 3 m and the sand content for the interval studied is about 80%.

Fault 16 shows a rather smooth SGR curve, with values between 7 and 30%. The total clay thickness in the fault varies between 2 and 12 mm. Fault 14 shows a higher variability in SGR values because the displacement is relatively small in comparison with the bed thickness. As already discussed in the section about clay smear, the total clay thickness in the fault gouge varies between 0 and 5 mm.

All the faults studied in the Airport road outcrop have a continuous clay seam over the interval studied, except when a sand layer is offset less than its thickness, and therefore has not moved past clay (SGR = 0). This means that although all faults in the Airport road outcrop have a relatively low SGR, the formation is compartmentalized (reduced permeability and capillary barriers for two-phase flow because of the presence of clay in the fault) because almost all faults are sealing, except for the SGR = 0 windows. We note that the probability of occurrence of SGR = 0 windows increases with increasing *N*/*G* ratio.

Fig. 16a is an attempt to find dependencies between SGR and some property of the clay gouge. Using the data shown in Fig. 15, together with data from faults 14 and 15, SGR was plotted against clay thickness, clay percentage (defined as clay thickness/total fault thickness) and fault thickness. A point-to-point correlation of SGR with one of the fault gouge parameters is not found, but the plot of the average SGR of the interval measured vs. the average clay content of the fault gouge for the same interval (Fig. 16b) shows that these average values are correlated. The relationship is described by the equation Clay (%) = 1.3*SGR. This means that in the Airport road outcrop on average we find 30% more clay in the fault gouge than expected from the percentage of clay in the faulted interval. This suggests that in this setting normal faults are in general enriched by clay, but we note that the number of faults measured in this study is too small to allow solid statistics.

Our observations that for nonzero SGR all faults contain a continuous clay smear contrast with the results of Yielding

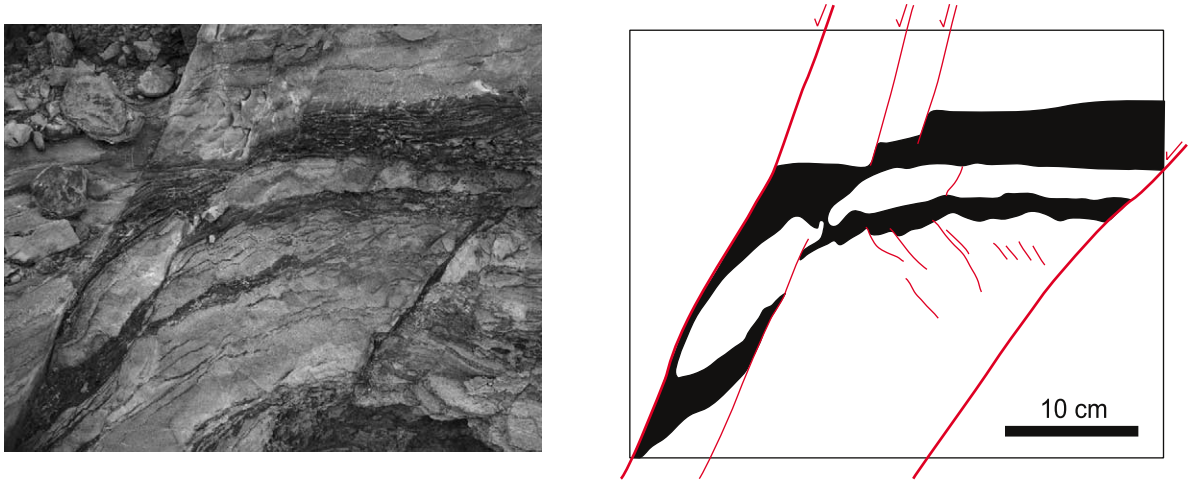

Fig. 13. Example of small-scale lateral clay injection inside the lens structure of fault 10. The clay layer is stepwise thinned towards the fault at the left. The clay is reallocated in the fault zone. The sandstone bed in the clay layer is disrupted, and is surrounded by clay.

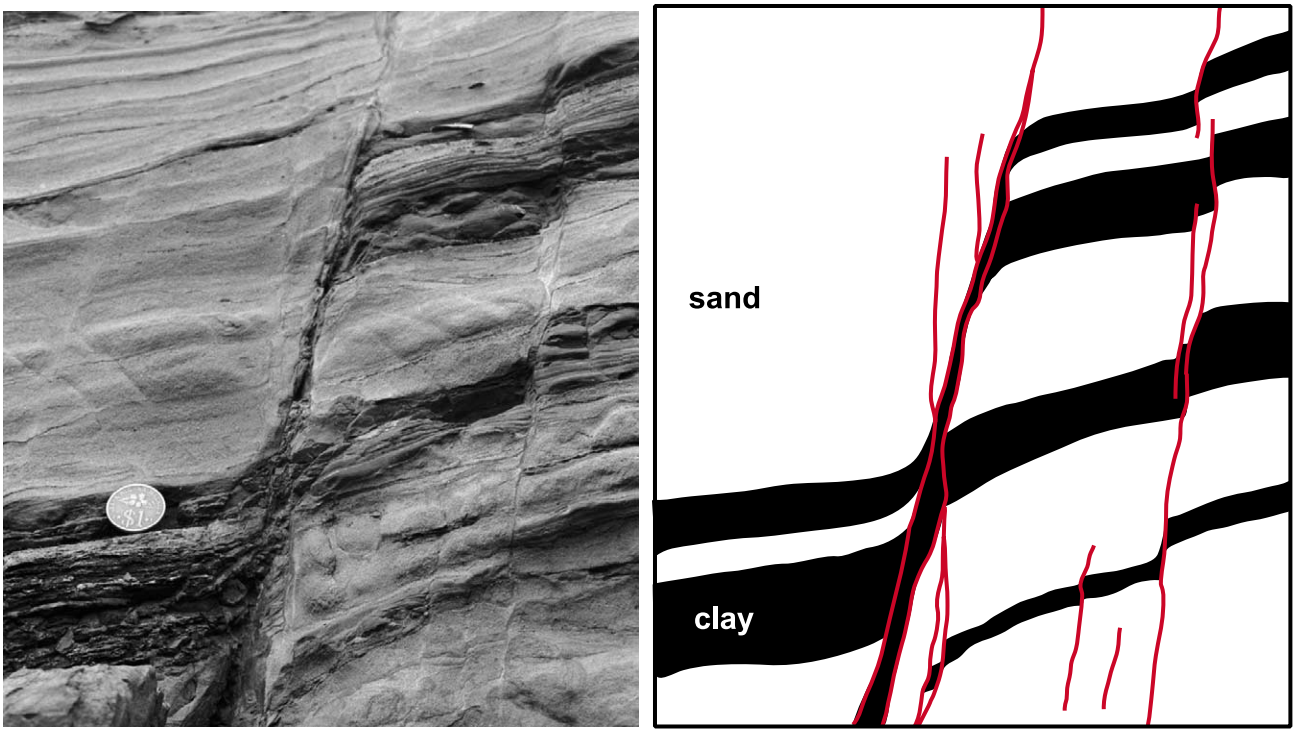

Fig. 14. Close-up of fault 8. The clay beds are sheared into the fault zone, and coalesce into a thick clay gouge. The sand beds are disrupted, but are not incorporated into the gouge. See text for discussion. Coin is approximately 2 cm.

(2002), which show that in many hydrocarbon accumulations, faults with SGR below approximately 20% do not seal or form continuous clay smear. This discrepancy may be explained in a number of ways. First (based on stereological arguments and the large number of observations), it is unlikely but cannot be excluded that the faults with a continuous clay gouge in profile may be discontinuous in 3D. Second, the processes operating in the faults at the Airport Road outcrop may be slightly different from those in the cases studied by Yielding (2002), for example caused by differences in mechanical properties (van der Zee et al., 2003), and in this setting faults are indeed sealing at very low SGR. Third, in subsurface studies the limits of resolution in evaluation of clay layers and small-scale fault structure may lead to errors in calculation of SGR. Yielding et al. (1997) reported that SGR analyses get more reliable when the throw of the fault is large. This is in agreement with our observation that average values show a better correlation. On one hand Fig. 16b seems to support this relationship and, on the other hand, we note that the variability depends strongly on the local structures in the fault (Vrolijk et al., 2005). Emphasis should be put on the prediction of local structures for further improvement of fault seal quantification tools.

6. Models of connectivity and juxtaposition

Fault zones consisting of two or more parallel strands (Childs et al., 1996a) have a major effect on across-fault juxtaposition and interpretation of connectivity analyses. This structure occurs at a wide range of scales from strands only a few millimeters apart up to hundreds of meters (Morley and Burhannudinnur, 1997). Interpretation of a fault as a single slip plane or as multiple strands is dependent on the scale of observation. For example two faults 10 m apart will be interpreted as one fault at seismic scale and in an outcrop as two separate faults (in a high resolution seismic dataset of the Airport road outcrop one could perhaps resolve two faults).

6.1. Influence on flow paths

An illustration of how two fault strands instead of one influence the across-fault fluid flow is shown in Fig. 17. This effect has been discussed previously by Childs et al. (1997). They showed, using an example from the upper Brent sequence, the influence of a double strand on juxtaposition analyses. It was assumed that both fault strands slipped 50% of the total fault throw. They found that, in the case studied, the double strand had a lower connectivity than the single strand case, but stated that this result was probably highly sequence dependent.

Building on the analysis of Childs et al. (1997), we carried out a series of simulations to quantify the effect of slip distribution on both strands for different layer thickness distributions. Our model (Fig. 18a) consists of a 100-m-thick sequence of five sand layers with interbedded clay.

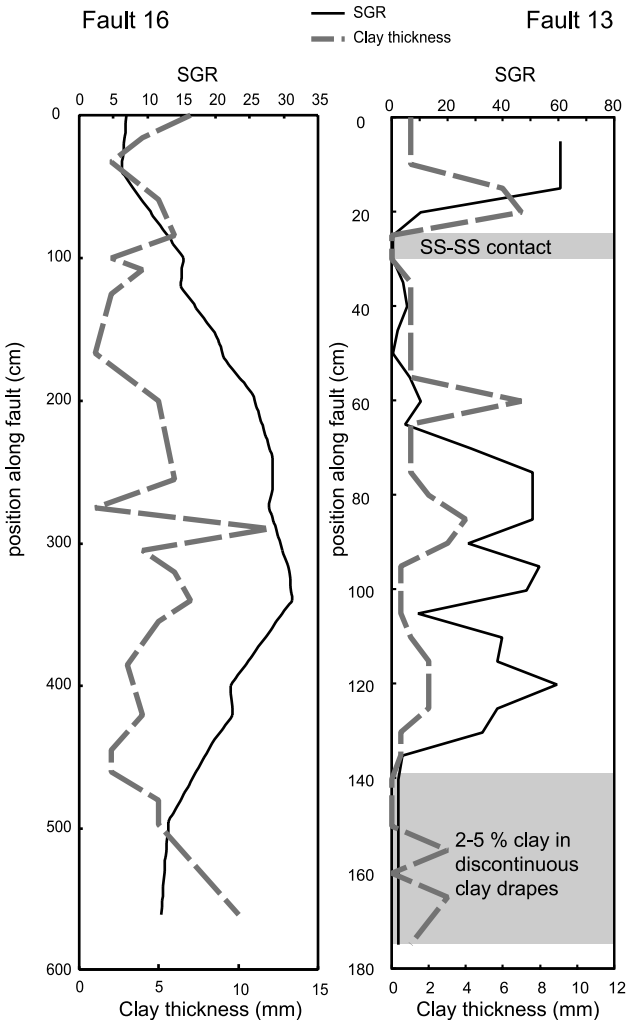

Fig. 15. SGR vs. clay thickness analyses for two faults, fault 16 (left) and fault 13 (right). No correlation between the two variables is found. Note that the only locations where clay is absent in the fault are in the sections where no clay has passed the sandstone. The lower layers in fault 13 have small clay drapes resulting in a SGR value of greater than zero, but with a lot of sand–sand windows where no clay has passed the sand.

This sequence is embedded in a shale formation that is thick enough to juxtapose the complete sequence against shale. The sequence was faulted along a fault consisting of two strands (fault 1) and (for comparison) along a fault of only one strand (fault 2).

The amount of throw was varied between 0 and 50 m. The distribution of throw over the two strands (t_1 and t_2 of fault 1 was varied in 0.5 m steps. For each combination of fault offset and slip distribution, the total across fault connectivity was calculated for both faults, assuming no sealing effects due to clay smear. Modeling the additional effect of clay smear is possible, for example by an additional SGR calculation, but this has not been included in this study. Clay layers are assumed impermeable. Details of the calculation are given in Appendix A.

The results of our simulations, normalized to the corresponding single-strand case (NACFAC, normalized across fault connectivity), are shown in Fig. 18b. We first illustrate the results for one specific combination of layers. In this figure, in a plot of throw on the left strand (t_1) against throw on the right strand (t_2) we contoured the values of normalized across-fault connectivity. It can be seen that there are combinations were the connectivity increases relative to one single strand (NACFAC>1), and in other combinations it decreases (NACFAC<1). The results appear non-systematic and one can expect the contours to depend on the combination of layer thicknesses chosen.

To investigate this, we analyzed different combinations of sand–clay ratios (the *N*/*G* ratio, the ratio of total sand thickness to the total thickness in a sequence) and layer thickness distribution, using a Monte Carlo simulation with uniformly distributed fault displacements. For every combination of layers, the maximum value of NACFAC was calculated for each value of the total throw. The result is the graph of Fig. 18c. On the horizontal axes *N*/*G* ratio and throw are plotted, and on the vertical axis a measure of the distribution of layer thickness (see Appendix A). The maximum values of NACFAC are plotted color-coded. This, admittedly complicated, diagram can be used to get an impression of the error made in a connectivity analysis, when the fault analyzed consists of two undetected strands.

6.2. Conclusion: telescoping along parallel strands

It can be concluded from these preliminary results that the reliability of juxtaposition diagrams can decrease dramatically in the presence of undetected multiple fault strands. The across-fault connectivity can either increase or decrease.

This effect is very difficult to predict accurately because it is sensitive to small variations in many of the input parameters. Fig. 18c shows the highly non linear behavior of our analysis. There are some trends, however: the effect is the smallest in sequences with a variable layer thickness and high *N*/*G* ratio. It is the largest in sequences with a constant layer thickness and a low *N*/*G* ratio.

To get an impression of the overall magnitude of this effect we prepared histograms of the minimum and maximum values of NACFAC obtained in each simulation. These are shown in Fig. 18d. It can be seen that for a significant part of the simulations the effect is small ($0.9<$ NACFAC<1.1). On the other hand, there are a large number of simulations with large variations.

7. Mechanics of fault-bounded lens shaped bodies

The formation of fault-bounded lens structures is related to the initially segmented nature of fault zones. Detailed study of a number of these structures in the field (cf. Fig. 9) has shown that the lens is invariably more deformed than the surrounding material. This observation can be explained in several ways. It is possible that most of the deformation

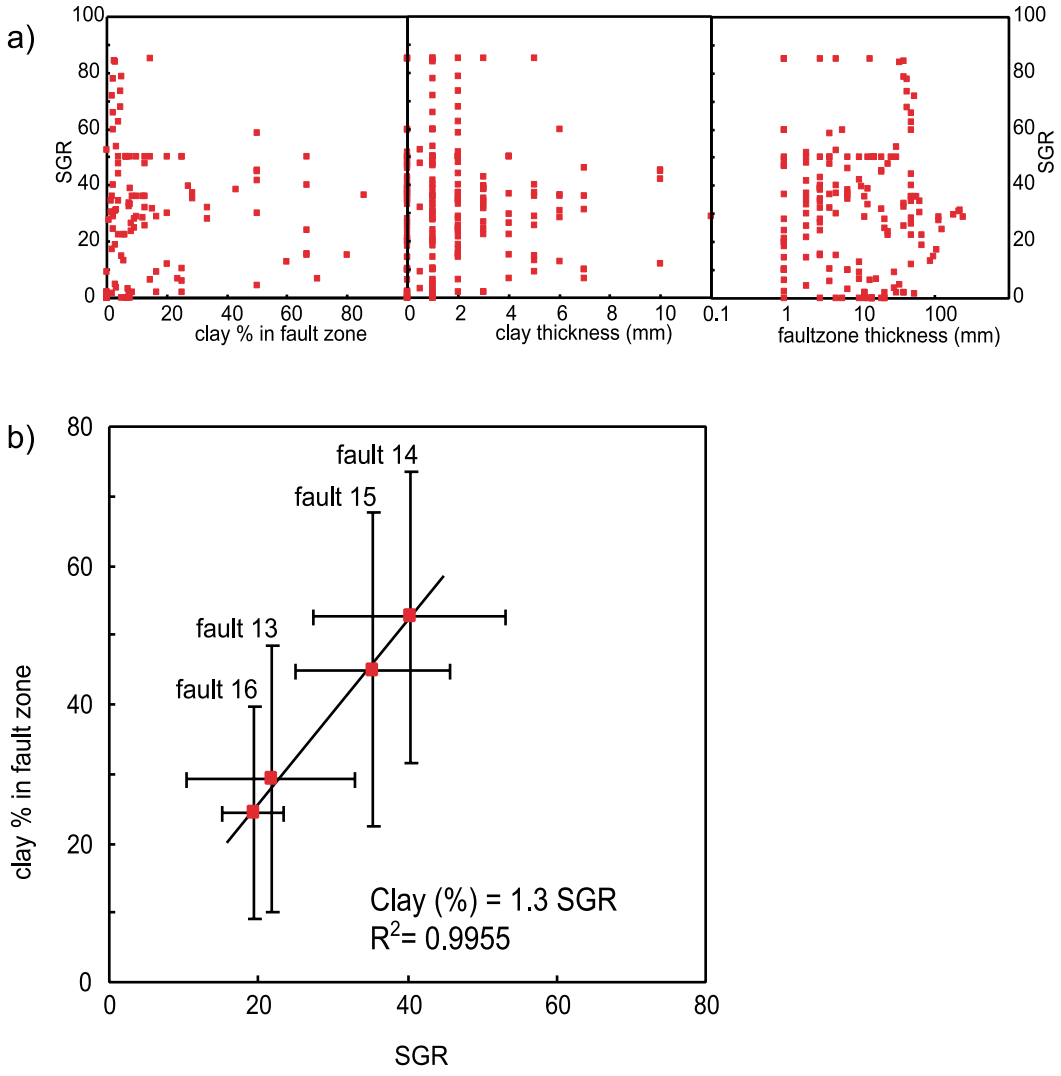

Fig. 16. (a) Combined data of faults 13–16. SGR is plotted vs. clay zone thickness, fault zone thickness, and clay percentage of the fault zone. No visible correlation is found. (b) Average values of SGR and clay percentage per fault show a good correlation: clay percentage = 1.3 SGR. The error bars are corresponding to the first standard deviation of each dataset.

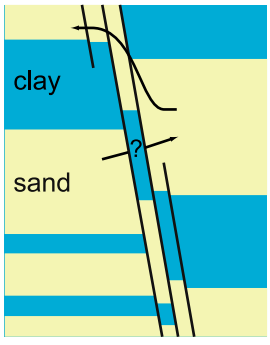

Fig. 17. Cartoon showing how the existence of more parallel slip planes increases the complexity and decreases the reliability of juxtaposition analyses. In the middle a sand–sand juxtaposition is blocked by a clay layer, whereas at the top, a clay top-seal is breached by a sand segment, forming a fluid pathway out of the system.

occurs before full coalescence of the slip planes and the formation of the lens (cf. Bürgmann and Pollard, 1994). Alternatively, the slip planes may coalesce and the lens may be formed before it deforms internally (Fig. 19). Here we ask the question if, in this second case, the redistribution of stresses in the structure can lead to preferential plastic deformation in the lens.

The reason why one can expect preferred deformation of the lens is illustrated with a strongly simplified cartoon (Fig. 20) of the stress changes in the region of a fault-bounded lens shaped structure in Mohr-space. The far-field initial stress state (1 in Fig. 20) is far from the peak strength failure envelope. With movement on the fault, the stress changes in the releasing and restraining bends. The main effect is that the horizontal stress in the releasing bend is reduced (2 in Fig. 20) where the vertical stress in the constraining bend is increased (3 in Fig. 20). In the interior

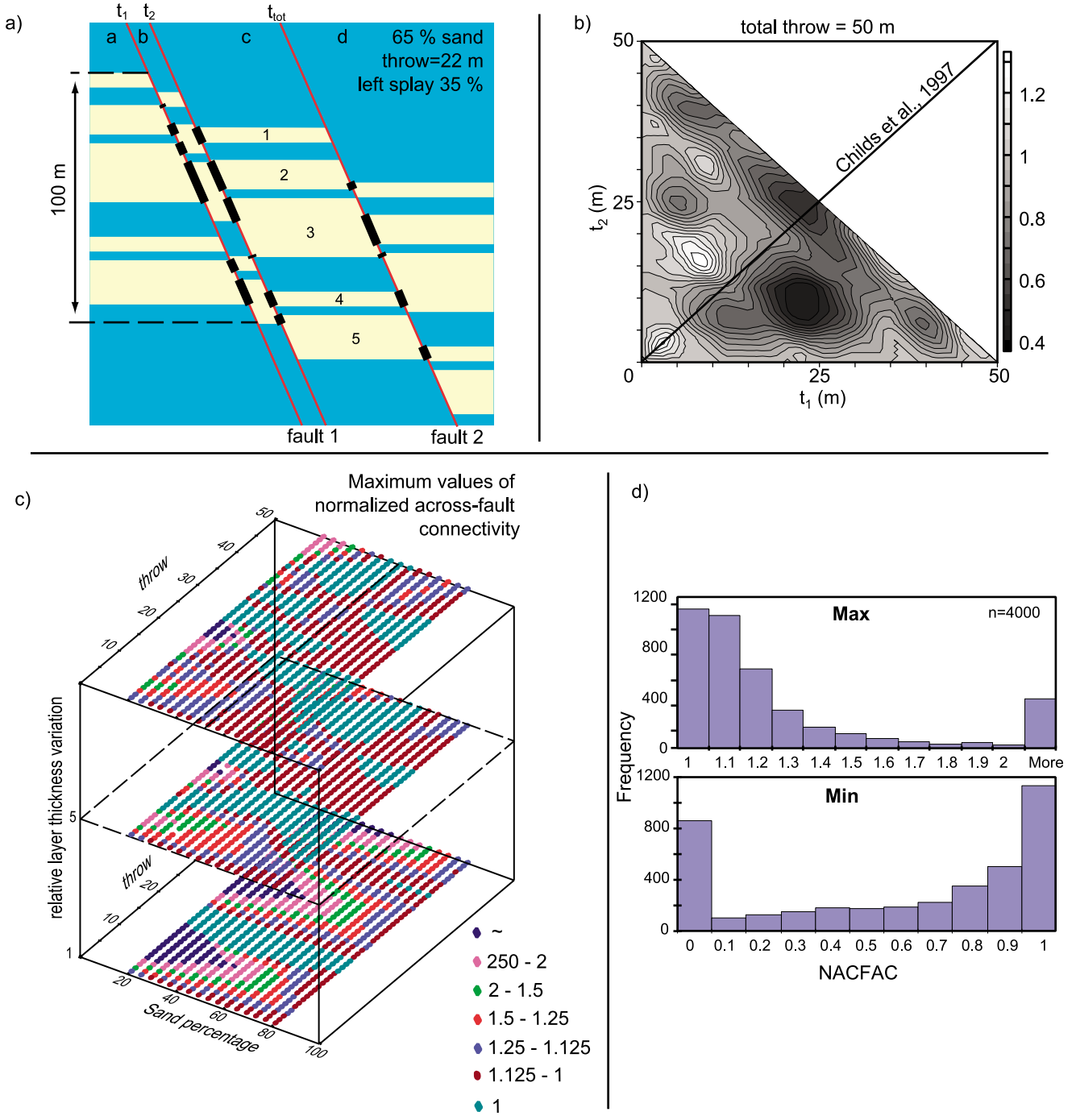

Fig. 18. Across-fault connectivity analyses. (a) Our model consists of a 100-m-thick (arrow) sequence with five sand and five clay layers. These are offset by two faults. Fault 1 consists of two parallel strands with throws t_1 and t_2 for each strand. Fault 2 consists of one strand with throw $t_{tot}(t_1+t_2)$. The *N*/*G* ratio and distribution is varied during the analyses. (b) A typical result for the example shown in (a). Axes are the throws t_1 and t_2, with the value of NACFAC (see Appendix A) contoured. This diagram can be compared with fig. 5d of Childs et al. (1997), which is a section through the diagram along the thin line indicated (albeit not normalized). (c) Plot of maximum values of NACFAC, in a plot with throw, *N*/*G* ratio and a measure for layer thickness variability (see Appendix A) on the axis. For each total throw the maximum value of NACFAC is determined (e.g. for $t_{tot}=50$ m, the maximum value on the diagonal line from top left to bottom right is taken). There are no clear trends recognizable. (d) Histogram of all maximum and minimum NACFAC values calculated in the analyses. Most values cluster between 0.9 and 1.1, but a significant number of large variations are also present.

of the lens, these changes are superposed, resulting in a decrease in horizontal stress and an increase in vertical stress. In the case sketched above, these stress changes are large enough to reach the peak strength in the interior of the lens, while outside the lens the increase in shear stress is smaller and the material does not reach the Mohr envelope (4 in Fig. 20).

To investigate this system in more detail, we constructed

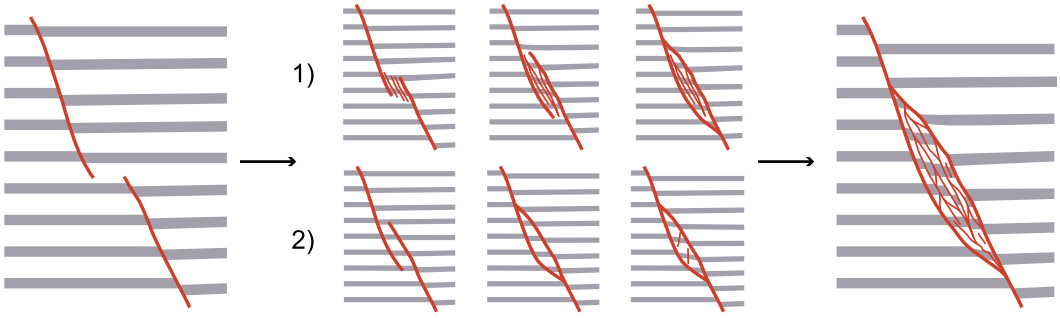

Fig. 19. Two scenarios for the development of fault-bounded lens-shaped bodies by coalescence of two non-planar faults. In scenario 1 the interior of the future lens is deformed before coalescence of the faults. Scenario 2 shows the fault coalescence before major deformation of the interior of the lens.

a finite element model. We model the effect of curved, predefined frictional discontinuities on the evolution of the stress field and plastic strain in an elasto-plastic medium in 2D. The wall rock has its intact strength everywhere and the fault has residual strength. In all analyses, the lens is symmetric. The length–thickness ratios investigated cover the range observed in the field. Full details of the analysis are given in van der Zee (2002).

The mechanical properties of the elasto-perfect-plastic material is as follows: Young's modulus of 50 GPa, Poisson's ratio of 0.3, cohesion is 10 MPa, and the internal friction angle is 20°. The high cohesion for the intact material and a cohesionless fault correspond to a depth of approximately 2 km, and an overconsolidated sediment that shows a drastic weakening after yielding. The model was deformed by a prescribed horizontal displacement of the upper boundary.

7.1. Modeling results

As expected, most of the displacement is accommodated on the faults; there are only very small displacement gradients in the continuum part of the model. Plastic deformation starts in the tip of the lens, propagating towards the center. To investigate the effects of the different parameters on the behavior of the model, we performed a series of analyses with different length–thickness ratios and with varying fault friction values, keeping all other input parameters constant. In all cases studied, plastic deformation is concentrated between the faults. In Fig. 21 we plot the results of these analyses in a matrix of the fault friction coefficient vs. the length–thickness ratio of the lens. For all combinations of length–thickness ratios and fault friction values, the magnitude of plastic strain is higher inside the lens structure than outside (Fig. 21).

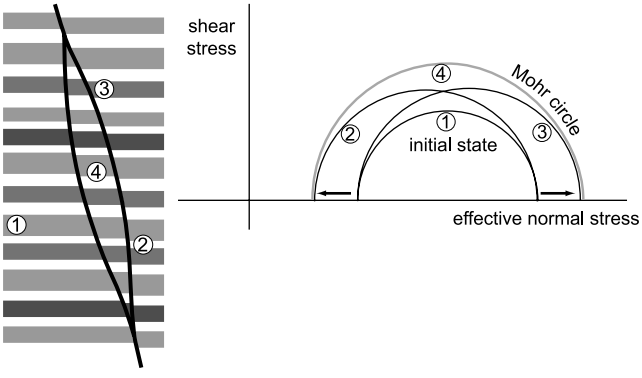

Fig. 20. Highly simplified geomechanical model for the preferred lens deformation illustrated in a Mohr diagram. The stress changes due to the slip along the lens, causes a preferred deformation of the lens interior. See text for discussion.

Detailed analysis of the results show that the smaller the length–thickness ratio of the lens, the more easily the stresses can be transmitted to its center. The first reason for this is purely geometric. Second, with a thicker lens the angle between the far-field maximum principle stress and the fault surface in the restraining bend increases. This orientation change causes an increase in normal stress on the fault, and this in turn causes an increase in friction at the fault plane. In other words, the orientation of the fault will be less favorable for slip than for the same position on a thinner lens. Comparing Fig. 21-2 with Fig. 21-8, we can see that model 2 with a length–thickness ratio of 4.4 shows a complete plastic interior of the lens, whereas model 8 (with a length–thickness ratio of 10) only shows plastic behavior in the lens tips, and not in the center of the lens (for the same total displacement).

The effect of fault friction is important because it determines the ratio of normal- and shear stress in the fault. In a frictionless fault, no shear stress can be transmitted. Comparing models 4 and 6 in Fig. 21, both lenses have the same length–thickness ratio ($L/T=8$), but different fault friction coefficients (0.25–0.4). With higher fault friction we observe plastic deformation in the center of the lens (model 6), but with the lower fault friction only the lens tips are deforming plastically (model 4).

7.2. Conclusions, preferred deformation fault-bounded lenses

Fault-bounded lens-shaped structures occur in most fault zones, at different scales. Our field data show that the

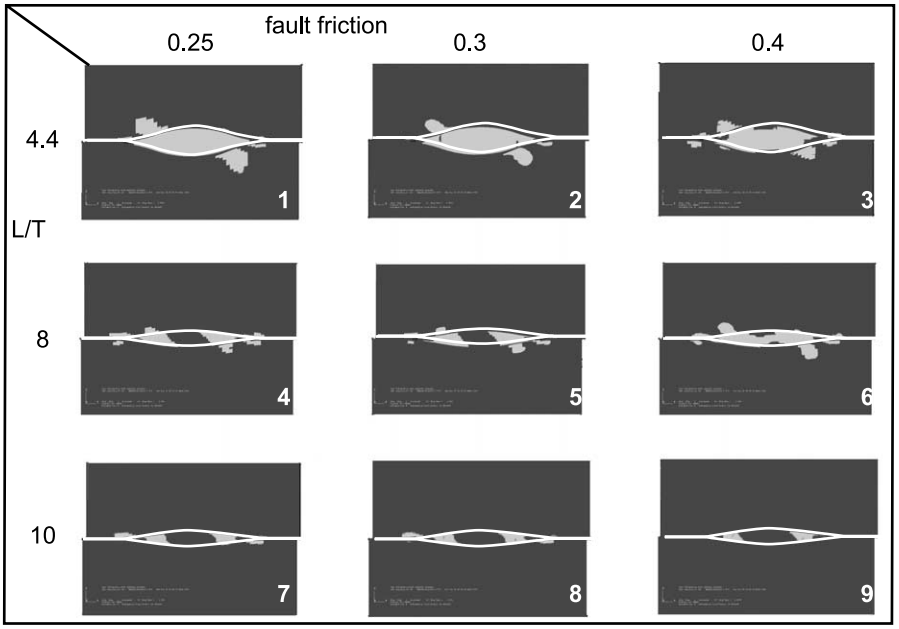

Fig. 21. Plots of plastic strain (gray are elements that have deformed plastically) in a length/thickness vs. fault friction coefficient matrix. Note that in all cases there is more deformation inside than outside the lenses. See text for discussion.

internal parts of the lenses are more deformed than the surrounding wall rock. This is consistent with the results of our numerical models, which show that, even for the case that the faults bounding the lens are formed before significant internal deformation, subsequent motion on the fault system will redistribute stresses in such a way as to initiate plastic deformation inside the lens. In other words, deformation in lenses inside fault zones can be expected to be higher than outside the zone. The finite element models show that in the initial stages of deformation the stresses evolve approximately in a manner similar to the highly simplified model shown in Fig. 20.

8. Conclusions

- The Airport road outcrop is an unique natural laboratory to study the complexities of normal fault systems. The relatively small bed-thickness combined with the throw of several times this bed thickness results in structures that can be considered as models of much larger structures offsetting thicker-bedded units.
- Down-dip segment linkage is one of the most important processes for fault growth. If the segments are not co-planar or have not the same orientation then additional deformation will take place with increasing offset.

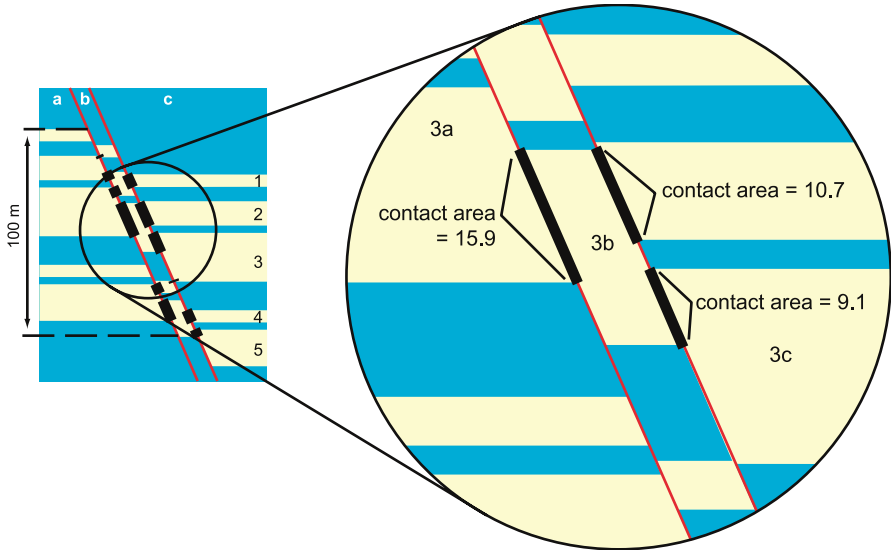

Fig. 22. Explanation of the across-fault connectivity algorithm used in Fig. 18. See text for further discussion.

Structures such as splays, short-cut faults, fault-bounded lens-shaped bodies and tectonic telescopes can develop. For an improved prediction of fault properties this is a key requirement.

- All faults studied have a continuous clay seam, except for the places where a sand bed has an offset smaller than its thickness, and therefore has not moved past clay.
- Several processes of clay incorporation into the fault gouge are identified (e.g. lateral clay injection and preferred smear). The clay content of the fault gouge does not show any correlation with individual SGR values, but a correlation between the average values of clay content and SGR over the whole fault is present.
- Connectivity analyses on a synthetic sequence show a decrease in reliability of juxtaposition diagrams in the presence of undetected multiple fault strands. The across fault connectivity can either increase or decrease, but exact prediction is hard to make. The general trends observed are that the smallest effect is in sequences with a variable layer thickness and a high *N*/*G*, and the largest effect is observed in sequences with a constant layer thickness and low *N*/*G* ratio.
- Field data show that the internal parts of fault bounded lenses are more deformed than the surrounding wall rock. Numerical models show that motion on the bounding faults will redistribute stresses in such a way that they initiate plastic deformation inside the lens. In other words, deformation in lenses inside fault zones can be expected to be higher than outside the zone.

Acknowledgements

Jown Tamaga and Danny Soo (Sarawak Shell Berhad) provided invaluable help with logistics in the field and discussions on many aspects of Airport Road geology. Careful and constructive reviews by Zoe Shipton and Chris Wibberley have helped to improve the manuscript. This project was funded by the Deutsche Forschungsgemeinschaft (UR 64-2).

Appendix A. Across-fault connectivity algorithm

The across fault connectivity for the two strands case was defined as follows. For each sand layer in the zone between the two strands, the length (in 2D) of contact of this layer with sand layers on each side was calculated. Of these two numbers, we take the smaller one to represent the connectivity contributed by this layer. This procedure is repeated for each sand layer in the zone between the two strands, and the total across fault connectivity for the two-strand case is calculated as the sum of these numbers. This is illustrated further in Fig. 22.

For example in the case of layer 3b, which has a contact area of 15.9 m with layer 3a and a total contact area of 19.8 m with layers 2c and 3c, the minimum was taken, which was 15.9 m. No clay smear effects were considered and therefore a 100% connectivity for sand–sand juxtapositions, and 0% connectivity for sand–shale or shale–shale juxtapositions were taken.

To allow comparison between simulations, the connectivity of the two strands case was normalized to the corresponding one strand case. In the case of Fig. 18, this means that the one strand case had a connectivity of 28.9, the two strands had a connectivity of 33.8, and therefore $33.8/28.9 = 1.17$ was taken as the normalized across-fault connectivity (NACFAC).

The measure for layer thickness variability is defined as the maximum layer thickness divided by the minimum layer thickness (in our model the sand layers are distributed as $1{:}x{:}2x-1{:}x{:}1$, with $1x5$, and the clay layers as $1{:}2x-1{:}x{:}2x-1{:}1$. This distribution does not cover all cases in nature and for more rigorous analysis this should be varied also).

References

Antonelli, M., Aydin, A., 1995. Effect of faulting on fluid flow in porous sandstones: geometry and spatial distribution. Bulletin of the American Association of Petroleum Geologists 79 (5), 642–671.

Beach, A., Welbon, A.I., Brockbank, P.J., McCallum, J.E., 1999. Reservoir damage around faults: outcrop examples from the Suez rift. Petroleum Geoscience 5, 109–116.

Bense, V.F., Van Balen, R.T., de Vries, J.J., 2003a. The impact of faults on the hydrogeological conditions in the Roer Valley Rift System: an overview. Netherlands Journal of Geosciences 82 (1), 41–54.

Bense, V.F., Van den Berg, E.H., Van Balen, R.T., 2003b. Deformation mechanisms and hydraulic properties of fault zones in unconsolidated sediments; the Roer Valley Rift System, The Netherlands. Hydrogeology Journal 11, 319–332.

Bouvier, J.D., Kaars-Sijpesteijn, C.H., Kluesner, D.F., Onyejekwe, C.C., van der Pal, R.C., 1989. Three-dimensional seismic interpretation and fault sealing investigations, Nun River Filed, Nigeria. AAPG Bulletin 73, 1397–1414.

Brown, S.R., Scholz, C.H., 1985. Broad bandwidth study of the topography of natural rock surfaces. Journal of Geophysical Research 90 (B14), 12575–12582.

Bürgmann, R., Pollard, D., 1994. Strain accommodation about strike–slip fault discontinuities in granitic rock under brittle-to-ductile conditions. Journal of Structural Geology 16 (12), 1655–1674.

Burhannudinnur, M., Morley, C.K., 1997. Anatomy of growth fault zones in poorly lithified sandstones and shales: implications for reservoir studies and seismic interpretations: part 1, outcrop study. Petroleum Geoscience 3, 211–224.

Caine, J.S., Evans, J.P., Forster, C.B., 1996. Fault zone architecture and permeability structure. Geology 24, 1025–1028.

Cartwright, J.A., Mansfield, C., Trudgill, B., 1996. The growth of normal faults by segment linkage. In: Modern Developments in Structural Interpretation, Validation and Modelling. Geological Society Special Publication 99, pp. 163–177.

Chester, F.M., Chester, J.S., 1998. Ultracataclasite structure and friction processes of the Punchbowl fault San Andreas system, California. Tectonophysics 295, 199–221.

Chester, F.M., Logan, J.M., 1986. Composite planar fabric of gouge from the Punchbowl Fault, California. Journal of Structural Geology 9, 621–634.

Childs, C., Walsh, J.J., Watterson, J., 1990. A method for estimation of the density of fault displacements below the limits of seismic resolution in reservoir formations. In: Buller, A.T., Berg, E., Hjelmeland, O., Kleppe, J., Torsaeter, O., Aasen, J.O. (Eds.), North Sea oil and Gas Reservoirs; II. Proceedings of the North Sea oil and Gas Reservoirs Conference. Graham & Trotman, London, pp. 309–318.

Childs, C., Watterson, J., Walsh, J.J., 1996a. A model for the structure and development of fault zones. Journal of the Geological Society, London 153, 337–340.

Childs, C., Nicol, A., Walsh, J.J., Watterson, J., 1996b. Growth of vertically segmented normal faults. Journal of Structural Geology 18 (12), 1389–1397.

Childs, C., Walsh, J.J., Watterson, J., 1997. Complexity in fault zone structure and implication for fault seal prediction. In: Møller-Pedersen, P., Koestler, A.G. (Eds.), Hydrocarbon Seals NPF special publication 7, pp. 61–72.

Clausen, J.A., Gabrielsen, R.H., Johnsen, E., Korstgård, J.A., 2003. Fault architecture and clay smear distribution. Examples from field studies and drained ring-shear experiments. Norwegian Journal of Geology 83, 131–146.

Crider, J.G., Peacock, D.C.P., 2004. Initiation of brittle faults in the upper crust: a review of field observations. Journal of Structural Geology 26, 691–707.

Develi, K., Babadagli, T., 1998. Quantification of natural fracture surfaces using fractal geometry. Mathematical Geology 30 (8), 971–998.

Fristad, T., Groth, A., Yielding, G., Freeman, B., 1997. Quantitative fault seal prediction: a case study from Oseberg Syd. In: Møller-Pedersen, P., Koestler, A.G. (Eds.), Hydrocarbon Seals NPF special publication 7, pp. 107–124.

Fulljames, J.R., Zijerveld, L.J.J., Franssen, R.C.M.W., 1997. Fault seal processes: systematic analysis of fault seals over geological and production time scales. In: Møller-Pedersen, P., Koestler, A.G. (Eds.), Hydrocarbon Seals NPF Special Publication 7, pp. 51–59.

Heynekamp, M.R., Goodwin, L.B., Mozley, P.S., Haneberg, W.C., 1999. Controls on fault-zone architecture in poorly lithified sediments, Rio Grande rift, New Mexico: implications for fault-zone permeability and fluid flow. In: Haneberg, W.C., Mozley, P.S., Moore, J.C., Goodwin, L.B. (Eds.), Faults and Subsurface Fluid Flow in the Shallow Crust Geophysical Monograph 113, pp. 27–49.

Holland, M., Urai, J.L., van der Zee, W., Konstanty, J., 2003. Fault gouge evolution in highly overconsolidated mudrocks—a field study. In: Proceedings, EAGE Conference on Fault and Top Seals, ISBN 90-73781-32-9, p. P42.

Hoogerduijn-Strating, E., Urai, J.L., 2003. Brittleness index—a tool to quantify the probability of dilatant fracturing in mudrock topseals. In: Proceedings, EAGE Conference on Fault and Top Seals, ISBN 90-73781-32-9, p. O20.

Ingram, G.M., Urai, J.L., 1999. Top-seal leakage through faults and fractures; the role of mudrock properties. In: Aplin, A.C., Fleet, A.J., Macquaker, J.H.S. (Eds.), Muds and Mudstone; Physical and Fluid-flow Properties Geological Society Special Publications 158, pp. 125–135.

Knipe, R.J., Fisher, Q.J., Jones, G., Clennell, M.R., Farmer, A.B., Harrison, A., Kidd, B., McAllister, E., Porter, J.R., White, E.A., 1997. Fault seal analysis: successful methodologies, application and future directions. In: Møller-Pedersen, P., Koestler, A.G. (Eds.), Hydrocarbon Seals NPF Special Publication 7, pp. 15–38.

Lehner, F., Pilaar, W., 1997. The emplacement of clay smears in syn-sedimentary normal faults: inference from field observations near Frechen, Germany. In: Møller-Pedersen, P., Koestler, A.G. (Eds.), Hydrocarbon Seals NPF Special Publication 7, pp. 39–50.

Lesslar, P., Wannier, M., 1998. Destination Miri—a geological tour northern Sarawak's national parks and giant caves: Ecomedia CD-Rom. http://www.sarawak.com.my/ecomedia_software

Lindsay, N.G., Murphy, F.C., Walsh, J.J., Watterson, J., 1993. Outcrop studies of shale smears on fault surfaces. Special Publications of the International Association of Sedimentology 15, 113–123.

Maltman, A., 1987. Shear zones in argillaceous sediments—an experimental study. In: Jones, M.E., Preston, R.M.F. (Eds.), Deformation of Sediments and Sedimentary Rocks Geological Society Special Publication 29, pp. 77–87.

Mansfield, C.S., Cartwright, J.A., 1996. High resolution fault displacement mapping from three-dimensional seismic data: evidence for dip linkage during fault growth. Journal of Structural Geology 18 (2/3), 249–263.

Martel, S.J., 1999. Mechanical controls on fault geometry. Journal of Structural Geology 21, 585–596.

McGrath, A.G., Davison, I., 1995. Damage zone geometry around fault tips. Journal of Structural Geology 17, 1011–1024.

Morgenstern, N.R., Tshalenko, J.S., 1967. Microscopic studies in Kaolin subjected to direct shear. Géotechnique 17, 309–328.

Morley, C.K., Burhannudinnur, M., 1997. Anatomy of growth fault zones in poorly lithified sandstones and shales: implications for reservoir studies and seismic interpretation: part 2, seismic reflection geometrics. Petroleum Geoscience 3, 225–231.

Mühlhaus, H.-B., Vardoulakis, I., 1987. The thickness of shear bands in granular materials. Geotechnique 37 (3), 271–283.

Navarro, M., 2002. Fault Roughness and Fault Complexity. PhD Thesis, University of Bonn, 96pp.

Neugebauer, H.J., 2003. Complexity of change and the scale concept in Earth System modeling. In: Neugebauer, H.J., Simmer, C. (Eds.), Dynamics of Multiscale Earth Systems. Springer, Berlin, pp. 41–63.

Peacock, D.C.P., Sanderson, D.J., 1994. Strain and scaling of faults in the chalk at Flambourgh Head, UK. Journal of Structural Geology 16 (1), 97–107.

Peacock, D.C.P., Knipe, R.J., Sanderson, D.J., 2000. Glossary of normal faults. Journal of Structural Geology 22, 291–305.

Power, W.L., Tullis, T.E., 1991. Euclidean and fractal models for the description of rock surface roughness. Journal of Geophysical Research 96 (B1), 415–424.

Ramsay, J.G., Huber, M.I., 1987. Folds and Fractures, The Techniques of Modern Structural Geology, vol. 2. Academic Press, New York. 391pp.

Rawling, G.C., Goodwin, L.B., Wilson, J.L., 2001. Internal architecture, permeability structure, and hydrologic significance of contrasting fault-zone types. Geology 29 (1), 43–46.

Schmitz, B., Urai, J.L., van der Zee, W., Holland, M., Littke, R., 2003. Transport properties and microstructural evolution in fault gouges—examples from a deltaic collapsed crest structure deformed at shallow depth. In: Proceedings, EAGE Conference on Fault and Top Seals, ISBN 90-73781-32-9.

Scruggs, V.J., Tullis, T.E., 1998. Correlation between velocity dependence of friction and strain localization in large displacement experiments on feldspar, muscovite and biotite gouge. Tectonophysics 295, 15–40.

Snoke, A.W., Tullis, J., Todd, V.R., 1998. Fault Related Rocks, A Photographic Atlas. Princeton University Press, Princeton, NJ. 617pp.

Urai, J.L., 1995. Brittle and ductile deformation of mudrocks. EOS November 7, F565.

Urai, J.L., Wong, S.W., 1994. Deformation mechanisms in experimentally deformed shales. European Geophysical Union Annual Meeting, Annales Geophysicae. Supp. 1 to Vol 12, P. C98.

Vrolijk, P., van der Pluijm, B.A., 1999. Clay gouge. Journal of Structural Geology 21 (8–9), 1039–1048.

Vrolijk, P., James, B., Myers, R., Maynard, J., Sumpter, L., Sweet, M., 2005. Reservoir connectivity analysis—defining reservoir connections and plumbing. SPE-93577, Proceedings of the 14th Middle East Oil and Gas Show, Bahrain, 12–15 March 2005.

Walsh, J.J., Watterson, J., 1993. Fractal analysis of fracture patterns using the standard box-counting technique: valid and invalid methodologies. Journal of Structural Geology 15 (12), 1509–1512.

Walsh, J.J., Watterson, J., Baily, W.R., Childs, C., 1999. Fault relays, bends and branch lines. Journal of Structural Geology 21 (8–9), 1019–1026.

Weber, K.J., Mandl, G., Pilaar, W.F., Lehner, F., Precious, R.G., 1978. The

role of faults in hydrocarbon migration and trapping in Nigerian growth fault structures. Proceedings of the 10th Annual Offshore Technology Conference.

Wibberley, C.A.J., Shimamoto, T., 2003. Internal structure and permeability of major strike-slip fault zones: the Median Tectonic Line in W. Mie Prefecture, S.W. Japan. Journal of Structural Geology 25, 59–78.

Willemse, E.J.M., 1996. 3D mechanics and evolution of discontinuous faults. PhD thesis, Stanford University, 236pp.

Willemse, E.J.M., Pollard, D.D., 2000. Normal fault growth: evolution of tipline shapes and slip distribution. In: Lehner, F.K., Urai, J.L. (Eds.), Aspects of Tectonic Faulting. Springer, Berlin, pp. 191–226.

Willemse, E.J.M., Peacock, D.C., Aydin, A., 1997. Nucleation and growth of strike–slip faults in limestone from Somerset, UK. Journal of Structural Geology 19 (12), 1461–1477.

Yielding, G., 2002. Shale gouge ratio—calibration by geohistory. In: Koestler, A.G., Hunsdale, R. (Eds.), Hydrocarbon Seals NPF Special Publication 11, pp. 1–15.

Yielding, G., Needham, G.T., Jones, H., 1996. Sampling of fault populations using sub-surface data. A review. Journal of Structural Geology 18 (2/3), 135–146.

Yielding, G., Freeman, B., Needham, D.T., 1997. Quantitative fault seal prediction. AAPG Bulletin 81 (6), 897–917.

van der Zee, W., 2002. Dynamics of fault gouge development in layered sand-clay sequences. PhD Thesis, RWTH Aachen. Shaker Verlag, ISBN3-8322-0585-3, 155pp.

van der Zee, W., Urai, J.L., Richard, P.D., 2003. Lateral clay injection into normal faults. GeoArabia 8 (3), 501–522.